DF-Laser Pulse Breakdown Induced by Maritime Aerosols

S.T. Amimoto,* J.S. Whittier,† F.G. Ronkowski,‡ P.R. Valenzuela,‡ G.N. Harper,‡ and R. Hofland Jr.§
The Aerospace Corporation, El Segundo, California

and

G.L. Trusty,¶ T.H. Cosden,** and D.H. Leslie¶
Naval Research Laboratory, Washington, D.C.

Thresholds for breakdown induced by liquid and solid aerosols in room air have been measured for a 1-μs-duration pulsed D_2-F_2 laser of 3.58-4.78 μm bandwidth. The DF laser beam was directed into an aerosol chamber that simulated maritime atmospheres on the open sea. For a focussed beam in which the largest encountered aerosol particles were of 1-4 μm diameter, pulsed DF breakdown thresholds were measured to lie in the range of 0.6-1.8 GW/cm². Salt-water aerosol breakdown thresholds for micron-size particles were found to be 15-30% higher than the corresponding thresholds for fresh-water particles. For a collimated beam that encountered particle diameters as large as 100 μm, breakdown could not be induced using 0.5 μs (FWHM) pulses at peak intensities of 59 MW/cm². Image converter camera measurements of plasma growth rates were obtained that compare favorably with earlier CO_2 measurements of Reilly et al. Pulsed DF breakdown thresholds of 32 MW/cm² for 30-μm-diam Al_2O_3 particles were also measured; these data agree with recent Lencioni high-frequency measurements if one assumes that the threshold for microsecond-duration pulses scales as λ^{-1}. An approximate theoretical model of the water particle breakdown process is presented that is found to be in satisfactory agreement with the experimental data and that allows scaling of the present results to other laser pulse durations, aerosol distributions, and transmission path lengths.

Nomenclature

dN/dR = aerosol particle number-density distribution function
E_i, E_t = laser energy incident upon and transmitted through breakdown region, respectively
I, I_B = laser intensity and centerline breakdown intensity, respectively
k = proportionality factor relating incident irradiance and detector output voltage
N = aerosol particle number density
$N(>R_0)$ = number density of aerosols with radii that exceed R_0
R = aerosol particle radius
r, θ, z = cylindrical coordinates
T = air plasma temperature
v_r, v_z = radial and axial velocities of expanding breakdown plasma, respectively
$w(z,t)$ = beam radius where laser intensity equals $e^{-1}I_0(t)$
γ = ratio of specific heats in air
ϵ_B, ϵ_c = laser fluence at breakdown and at centerline, respectively
λ = laser wavelength
ρ = air mass density
τ_B, τ_c, τ_p = times for onset of breakdown formation, laser beam cutoff, and laser duration, respectively

Presented as Paper 82-0894 at the AIAA/ASME Third Joint Thermophysics, Fluids, Plasma, and Heat Transfer Conference, St. Louis, Mo., June 7-11, 1982; submitted June 17, 1982; revision received Oct. 5, 1983.

*Member of the Technical Staff, Mechanics Research Department, Aerophysics Laboratory.

†Head, Mechanics Research Department, Aerophysics Laboratory. Member AIAA.

‡Laboratory Technician, Mechanics Research Department, Aerophysics Laboratory.

§Senior Staff Scientist, Aerophysics Laboratory. Associate Fellow AIAA.

¶Research Physicist, Optical Sciences Laboratory.

**Electronics Development Technician, Optical Sciences Laboratory.

Introduction

LASER plasma ignition by aerosol particles limits the optical intensities that can be propagated through the atmosphere. Above the breakdown threshold, aerosol particles ignite intense plasmas that have high extinction to visible and infrared irradiation. These plasma grow rapidly and may fully block the laser beam, depending upon the number density of the breakdowns, the plasma radial growth rate, and the laser pulse duration. Previous experimental and theoretical work on the aerosol-induced breakdown problem has been carried out primarily at CO_2 laser wavelengths (10.6 μm),[1-6] in which it was shown that 1) aerosol particles lower the breakdown threshold below the clean air value; 2) threshold reduction is relatively insensitive to aerosol particle material, except for the case of water aerosols that cause a significantly smaller reduction in threshold than do solid-particle aerosols; and 3) for large-diameter particles, the breakdown threshold decreases with both increasing particle size and increasing laser pulse duration. The case of multiple-pulse propagation through liquid and solid aerosols at CO_2 wavelengths has been studied experimentally and theoretically by Reilly et al.[7] At pulsed, high-frequency (HF) chain-laser wavelengths, thresholds for air breakdown initiated by various solid aerosols have been measured using a long pulse duration (3.5 μs) laser beam.[8] Measured thresholds were found to be higher by factors of 3-5 than the corresponding 10.6 μm data, suggesting a breakdown threshold dependence on wavelength of $I_B \sim \lambda^{-1}$. This result contrasts sharply with short-pulse data[5,9] where the threshold for large particles has been found to scale as λ^{-2}. Recently, a pulsed DF-laser threshold measurement has been reported for clean helium[10]; earlier, short-pulse HF and DF laser breakdown of air was studied by two groups.[11,12] Aside from that work, we are aware of no breakdown data that have been published at the laser wavelengths employed in the present study.

This paper describes the results of a brief (three-week) experimental study of long-pulse breakdown induced by simulated maritime and solid-particle aerosols at pulsed-DF chain-laser wavelengths (3.58 − 4.78 μm). Threshold measurements in maritime aerosols have been performed using both

collimated and focussed beams, bracketing the intensity range of breakdown-free propagation over long transmission paths. Radial and axial growth rates of the aerosol-initiated plasmas have also been measured. An approximate theoretical model of the aerosol breakdown process that considers aerosol vaporization and subsequent cascade ionization by the laser beam is shown to be in reasonable agreement with the experimental data and, in principle, allows scaling of the laboratory breakdown data to long propagation paths.

Experimental Technique

A magnetically confined electron beam was used to initiate the pulsed chain-reaction DF laser.[13] Mixtures containing 20% F_2/8% D_2 by volume were irradiated for periods of approximately 0.5 μs at current densities of 20 A/cm^2 to accomplish laser initiation. Nominal laser energies of 30 J in 0.8 μs (FWHM) pulses were delivered at cavity pressures of 800 Torr. Laser energy and pulse duration variations were accomplished through adjustment of the laser cavity pressure. Energy was extracted from the gain medium by means of a transmission-coupled half-symmetric unstable resonator and then collimated using a CaF_2 lens of 8-m focal length. Burn patterns on calibrated witness film indicated a highly uniform intensity profile in the near-field output beam. The beam was propagated a distance of about 100 m from the laser facility through an insulated duct to the vicinity of the aerosol generator.

The experimental configuration in the area of the aerosol chamber is shown in Fig. 1. Two CaF_2 wedges were used to sample the incident and transmitted laser energy and irradiance time history on each breakdown experiment. Laser pulse energies were measured using ballistic thermopiles, and emission time profiles of the laser pulse were monitored with Au : Ge detectors. Both collimated and focussed beams were directed into the aerosol chamber. A 3 : 1 reducing telescope consisting of a 3 m radius concave mirror and a 1 m radius convex mirror was used to generate a collimated beam. Substitution of a flat mirror for the convex mirror element in the telescope permitted the laser beam to be brought to a focus within the aerosol generator.

Three techniques were employed in the observation of aerosol breakdowns. An open-shutter camera was used to provide unequivocal photographic evidence of breakdown in the aerosol chamber. The onset of ultraviolet emission from breakdown plasmas was monitored using a 1P28 photomultiplier tube. Rapid cutoff of the transmitted DF beam was observed to follow closely the onset of uv plasma emission. This sequence of events is illustrated in the oscillograms of Fig. 2. For the case shown, full beam blockage is seen to occur in the transmitted irradiance record (middle trace) approximately 100 ns after the ultraviolet emission record (lower trace) shows first evidence of plasma formation (1.5 μs). Aerosol plasma growth rates were obtained using image converter camera data. Framing rates of 10^6 or 2×10^7 s^{-1} were employed; exposure time at 20 MHz framing speed is 10^{-8} s. A discussion of the data obtained with the image converter camera is presented later.

The spatial distribution of radiation in the breakdown region was determined using burns on exposed, developed photographic film.†† For the focussed beam case, a Gaussian intensity distribution, $I(r,z,t) = I_0(t)\exp[-(r/w)^2]$, was assumed, and from the burns we determined w. The centerline fluence ϵ_c was calculated from the measured pulse energy E_p and w according to the relationship

$$\epsilon_c = \epsilon(r=0,z) = \lim_{r\to 0}\int_0^\infty I(r,z,t)\,dt = \frac{E_p}{\pi w^2(z)} \quad (1)$$

††A 64-element array is being employed to obtain precise information about the laser-fluence spatial distribution in the focal volume; initial results with the array appear to corroborate use of the approximate burn technique employed in the present study.

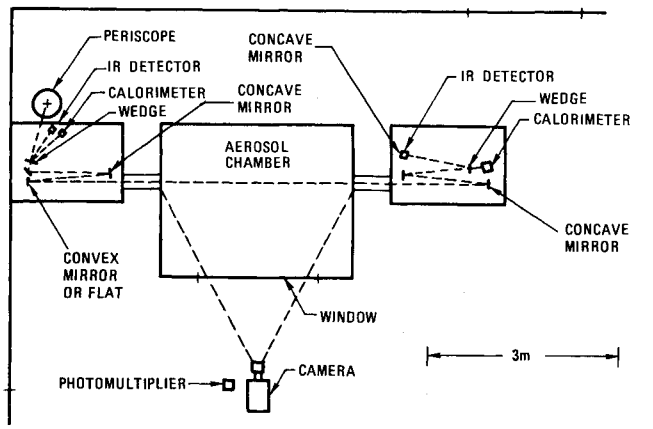

Fig. 1 Experimental arrangement in aerosol chamber laboratory.

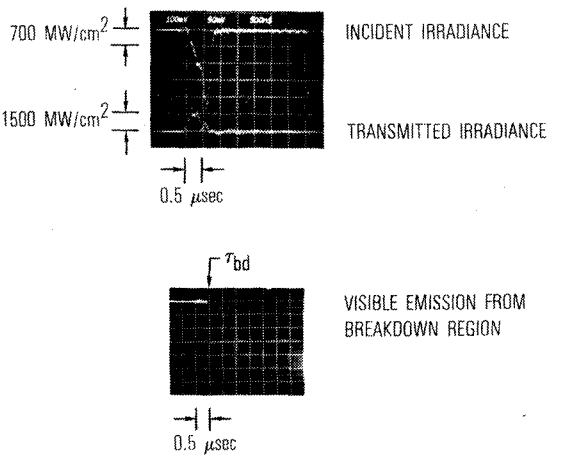

Fig. 2 Oscillograms of incident irradiance, transmitted irradiance, and plasma ignition onset.

The centerline intensity at breakdown was determined from the expressions

$$I_B = I(r=0,z,t_B) = kv(t_B) \quad (2)$$

$$k = \epsilon_c \Big/ \int_0^\infty v(t)\,dt \quad (3)$$

where k (W/cm^2 · V) is the proportionality factor relating the incident irradiance and the detector output voltage and t_B is the time to breakdown as determined from the photomultiplier measurement of plasma emission onset. The accumulated centerline fluence at breakdown was obtained from the equation

$$\epsilon_B = \epsilon(r=0,z,t_B) = \int_0^{t_B} I_0(t)\,dt \quad (4)$$

The irradiance waveforms were digitized to perform numerical evaluation of the integrals in Eqs. (3) and (4). For the collimated beam (near-field) case, the transmission-coupled unstable resonator produced a nearly uniform spatial fluence and irradiance distribution such that $\epsilon_c \cong \bar{\epsilon} = E_p/A_{\text{burn}}$ and $I_0 \cong \bar{I} = kv(t)$. A film burn that illustrates the uniformity of the resonator near-field fluence distribution is shown in Fig. 3.

An aerosol generator was used to simulate representative maritime and fog bank conditions on the open ocean.[14] A $3.6 \times 2.3 \times 2.1$ m metal enclosure was internally fitted with four nozzle heads and three spinning disk humidifiers for dispensing salt- or fresh-water aerosols. After a transient period of about 30 min, it was found that a temporally stable

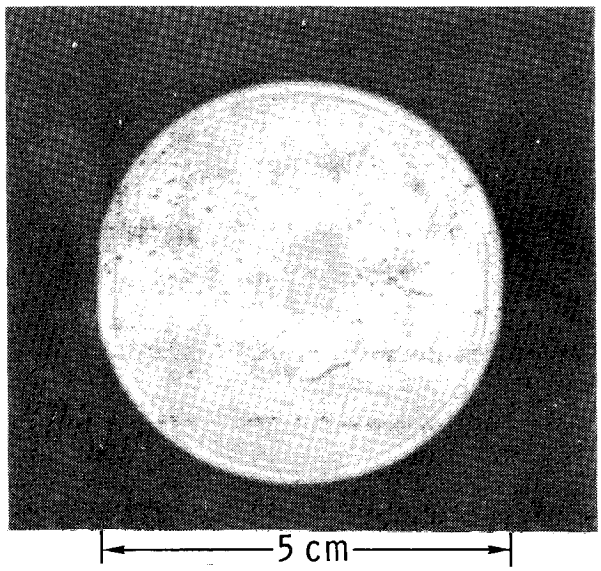

Fig. 3 Near-field burn of pulsed DF laser output.

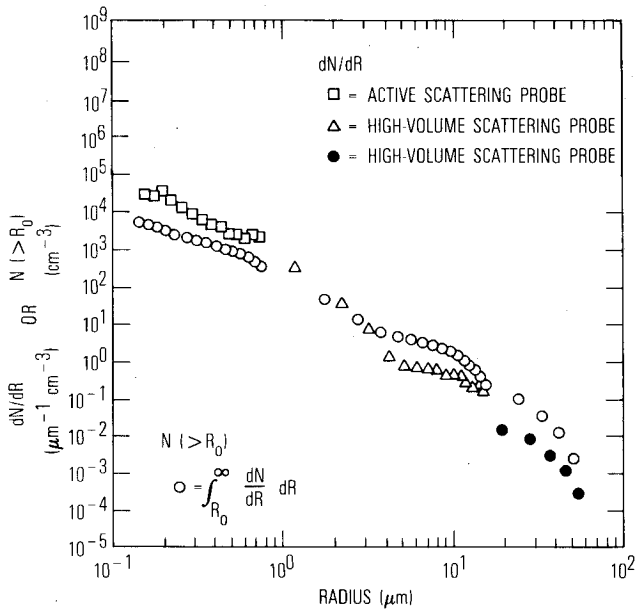

Fig. 4 Aerosol size distribution measurement for fog-like maritime environment.

distribution could be achieved. Relatively uniform spatial aerosol distributions within the enclosure were obtained by use of a circulation fan. The enclosure was fitted with ports on three of its sides that were opened several seconds before an experiment to permit laser beam and camera access to the particle-laden air. Three particle spectrometers were installed within the chamber to sample aerosol size distributions between 0.1 and 200 μm. Data from the sensors were recorded on magnetic tape at 1 s intervals and fed to a PDP-11/34 data acquisition system for real-time processing. Output from the computer included aerosol size distributions from the probe data and the calculation of particle number density. An actual probe measurement and calculation using the above system is illustrated in Fig. 4 for the case of a fog bank simulation by the aerosol generator. The plot presents dN/dR (cm^{-3} μm^{-1}), where N is the particle concentration and R the particle radius, vs R using logarithmic coordinates. The "squares" in Fig. 4 indicate the range of the active scattering probe, and the "triangles" and "solid circles" indicate the ranges of the two high-volume scattering probes. Also included in Fig. 4 is a calculation of $N(>R_0)=\int_{R_0}^{\infty} dR\, dN/dR$,

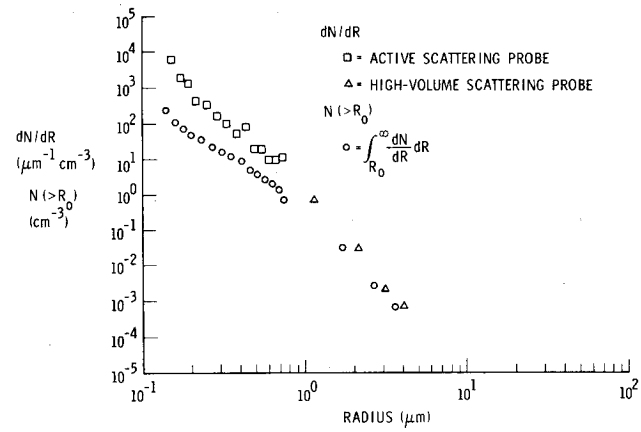

Fig. 5 Aerosol size distribution measurement for typical maritime environment.

the number density of particles with radii that exceed R_0. Figure 5 illustrates the results of probe measurements of an aerosol distribution that closely simulates a maritime condition of the type reported in Ref. 14. In general, breakdown measurements were carried out in the fog bank aerosol distributions illustrated in Fig. 4.

For solid-particle aerosol breakdown experiments, a nitrogen gas-driven fluidized-bed injector was constructed to produce a uniform Al_2O_3 aerosol suspension. Alumina particles of 20 μm diam were selected for use with the air-driven aerosol generator. Aerosol density in the breakdown region was sufficiently large to provide numerous Al_2O_3 particles in the focal volume, but small enough that diffractive fill-in was insured.

Results and Discussion

The breakdown measurements carried out during the present study are summarized in Table 1. The values of breakdown threshold I_B correspond to those values of centerline irradiance at the focal plane which give a high probability (~ 90%) of breakdown. The accumulated fluence at the time of breakdown is also shown for cases where an unequivocal determination of breakdown time could be made. The estimated uncertainty in the reported thresholds is $\pm 30\%$. The error is dominated by the uncertainty in the spatial beam profile at the breakdown location.

For the collimated beam case shown in Table 1, we were unable to achieve breakdown at peak centerline intensities of 59 MW/cm^2 in a fog-like aerosol distribution. From the extrapolated aerosol distribution function, the largest particle diameter in the irradiated volume was calculated to be 100 μm. During this experiment, the laser intensity exceeded 50 MW/cm^2 for a 500 ns portion of the pulse. Assuming the threshold scales as $\tau_p^{-0.5}$, we infer a safe intensity for a $t(\mu s)$ duration pulse propagating through aerosols of 100 μm diam or smaller to be 35 $[t(\mu s)]^{-0.5}$ MW/cm^2.

Breakdown experiments were performed using 20-μm-diam Al_2O_3 particles suspended in the focal region of the DF beam in order to gain confidence in the present experimental technique. A 4.5 μs (FWHM) laser pulse was employed for these breakdown tests. The measured threshold of 32 MW/cm^2 shown in Table 1 is plotted in Fig. 6 along with the recent long-pulse (3.5 μs) data of Lencioni at HF and CO_2 wavelengths.[4,8] Assuming that λ^{-1} scaling is valid in the present regime, the present threshold measurement is seen to be in excellent agreement with the experimental results of Lencioni et al.

Two kinds of breakdown experiments are summarized in Table 1 for fog-like distributions and focussed beams. In the first class of experiments (runs 727 and 742), the laser cavity pressure and, consequently, the pulse energy were reduced in

Table 1 Aerosol breakdown summary

Run	Aerosol	Beam	Volume, cm^3	Largest Part. diam, μm	t_B, μs	I_B, MW/cm^2	ϵ_B, J/cm^2
712	Fog (fresh)	Collimated	110	102	$>\frac{1}{2}$	> 59	> 39
727	Fog (fresh)	Focussed	8×10^{-3}	1.5	—	620	—
742	Fog (salt)	Focussed	8×10^{-3}	2.6-4	0.41-1	710-855	—
758	Al_2O_3	Focussed	8×10^{-3}	20	—	32	—
778	Fog (fresh)	Focussed	8×10^{-3}	1.5	0.4	1605	320
779	Fog (fresh)	Focussed	8×10^{-3}	1.5	0.39	1850	795
780	Fog (fresh)	Focussed	8×10^{-3}	1.5	0.41	1640	475

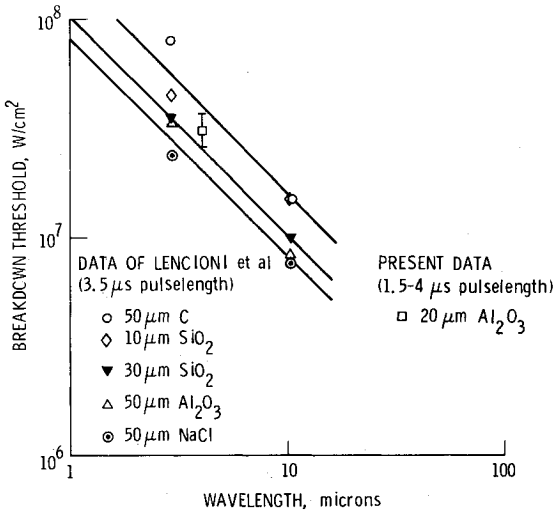

Fig. 6 Present measurement of alumina breakdown threshold compared with data of Lencioni et al.

small increments, using temporally flat-topped laser irradiance profiles, until breakdown was observed to cease. This approach yielded the smallest measured values of breakdown threshold. Note in Table 1 that the threshold for salt-water aerosols is somewhat higher than that for fresh-water aerosols, even though larger particle sizes were sampled in the salt-water aerosol case. In the second class of experiments (runs 778-780), the laser was operated at 800 Torr cavity pressure, yielding peak irradiances that were at least five times higher than the previously measured breakdown thresholds. In this class of experiments, breakdowns were observed at times for which the incident irradiance was still increasing rapidly with time (Fig. 2). The intensities at which breakdowns were observed in these experiments were approximately 2.5-3 times greater than the values measured by the prior method. The fact that significant differences were observed in measured breakdown thresholds for the two classes of pulses was not unexpected. The situation can be described with the aid of Fig. 7 in which scaled drawings of flat-topped and fast-rising waveforms are superimposed. The fast-rising waveform of Fig. 7 is obtained from the oscillogram of incident irradiance in Fig. 2 (run 778). The flat-topped waveform is sketched from the oscillogram of incident irradiance for run 727. Inspection of Fig. 7 yields the breakdown threshold for the fast-rising pulse as

$$I_B' = I_B + \frac{dI}{dt}(\tau_B' - \tau_0)$$

where I_B' and I_B are the breakdown thresholds for the fast-rising and flat-topped pulses, respectively, τ_B' the time to attain breakdown for the fast-rising pulse, and dI/dt the time rate of irradiance rise for the fast-rising laser pulse. The theory of Ref. 15 has been used to calculate times for vaporization and plasma ignition for the waveforms of Fig. 7. Calculated breakdown times for the flat-topped and fast-rising pulses are

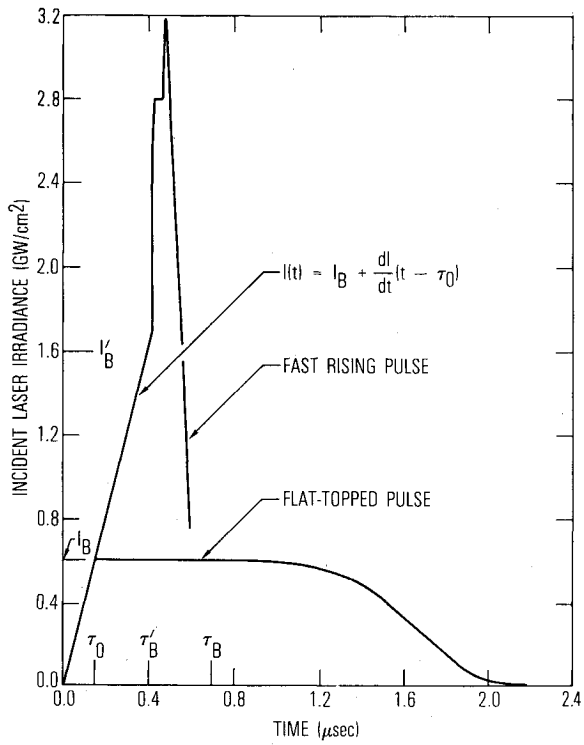

Fig. 7 Laser irradiance vs time for flat-topped and fast-rising pulses.

$\tau_B = 705$ ns and $\tau_s' = 390$ ns, respectively; good agreement with the measured time to breakdown for run 778 is observed. The breakdown time for the fast-rising pulse is significantly shorter than that of the flat-topped pulse because of the higher effective intensity acting during the vaporization and avalanche ionization phases of the fast-rising pulse. Calculated breakdown threshold for the fast-rising pulse of 1.7 GW/cm^2 follows from the above equation with $dI/dt = 4.25$ $MW/cm^2/ns$, $I_B = 0.6$ GW/cm^2, and $\tau_B' - \tau_0 = (390 - 140)$ ns. Calculated threshold is close to the measured threshold of 1.6 MW/cm^2 for run 778. Thus, significant quantitative differences in the breakdown threshold of fast-rising and flat-topped pulses have been explained on the basis of theoretical considerations. In general, an appreciable difference in breakdown threshold between fast-rising and flat-topped pulses will be observed when the laser rise time satisfies the inequality $dI/dt \geq I_B/\tau_B$, as in the present case. The present data highlight the important role that the laser pulse shape plays in the determination of a threshold value for the breakdown irradiance.

The breakdown irradiance data of Table 1 are plotted in Fig. 8 as a function of aerosol particle diameter. Included in Fig. 8 are the recent long-pulse HF data of Lencioni et al.[8] and an unpublished theoretical breakdown calculation[15] that extends the treatment of Smith[16] to include electron attachment to water vapor and molecular oxygen. Briefly, the vapor

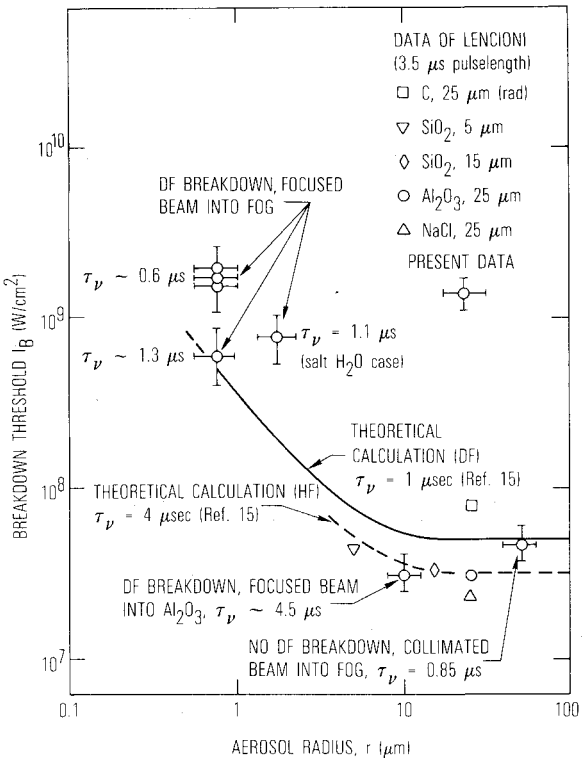

Fig. 8 Pulsed chemical laser breakdown threshold vs aerosol size: theory and experiment.

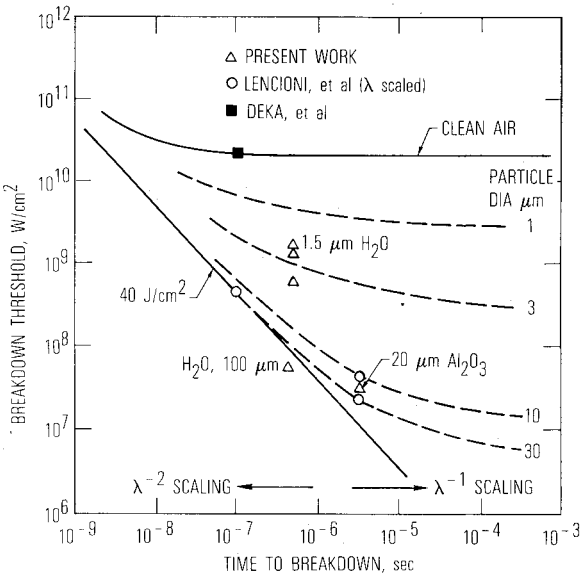

Fig. 9 Estimated air breakdown thresholds for DF laser pulses.

density leaving the aerosol surface as a result of laser irradiation of the particle is determined in the model, and the intensity required to cascade ionize the vapor to complete ionization is calculated. Qualitatively speaking, smaller particles are more difficult to ionize because of their low absorption efficiency and high rate of electron loss by free and ambipolar diffusion. For aerosol particles larger than 7 μm, elastic heating and attachment losses dominate over diffusion losses under present conditions. The predicted DF threshold for nominal 1 μs duration pulses is plotted in Fig. 8 as the solid curve, while the dotted curve is the predicted HF threshold for nominal 4 μs long pulses. The agreement between theory and experiment is considered satisfactory considering the simplified nature of the model and the experimental error in the determination of particle size and breakdown threshold.

The data of Fig. 8 have been used to construct an empirical map in Fig. 9 of DF breakdown threshold as a function of particle size and time-to-breakdown. Implicit in the construction of Fig. 9 is the assumption that the DF thresholds are relatively insensitive to particle material as has been found to be the case at HF and CO_2 wavelengths. Included in the figure are the DF clean-air breakdown data of Deka et al.[11] and the results of our wavelength scaling of the data of Lencioni et al.[5,8] Considerable liberty has been taken in estimating the position of the curves according to particle size. It should be emphasized that much additional data must be generated before the empirical correlation of Fig. 9 has a firm experimental basis for DF wavelengths.

A typical series of image converter frames that depict the breakdown spatial growth rate at intensities above the breakdown threshold is shown in Fig. 10. The dashed lines in the frames mark the e^{-1} diameter of the laser beam, which we estimate to be 1.6 mm. The laser pulse is incident from the bottom of Fig. 10. Two breakdowns can be observed in the first two frames. The lower breakdown starts near the center of the beam and grows radially to completely fill the beam after about three frames. The inferred radial expansion velocity is consistent with the observed delay time between the cutoff of the transmitted laser pulse and the initial observation of plasma ignition. As time progresses, the upper breakdown plasma is shielded by the lower breakdown; it is completely extinguished by the third frame. The lower breakdown plasma is observed to form an inverted-pyramid-like shape as it selectively absorbs radiation at its front surface and propagates back toward the laser source. This behavior is characteristic of a laser-supported detonation (LSD) wave.[17]

Radial and axial velocities of the expanding breakdown plasmas have been calculated from the experimental data of Fig. 10. These results are presented in Fig. 11 along with data obtained at CO_2 wavelengths.[18] Included in Fig. 11 are the theoretical predictions of Raizer for the radial and axial plasma growth rates. Although the data lie somewhat above the predicted velocities, agreement between theory and experiment is considered reasonable. At 1 GW/cm² irradiance, we estimate the plasma specific energy to be[17]

$$\epsilon = \frac{\gamma(I_0/\rho_0)^{\frac{2}{3}}}{(\gamma^2-1)^{\frac{1}{3}}(\gamma+1)} = 2.9\times 10^{12}\ \text{erg/g} \qquad (5a)$$

and the plasma temperature to be[19]

$$T = 0.86\left(\frac{\rho}{\rho_0}\right)^{0.08}\left[\frac{\epsilon(\text{eV/molec})}{8.3}\right]^{\frac{2}{3}} = 4.2\ \text{eV} \qquad (5b)$$

The extension of the present laboratory-scale results to long-path transmission in the atmosphere has been numerically studied following standard formulations. An example serves to illustrate the parameter regime where blockage by

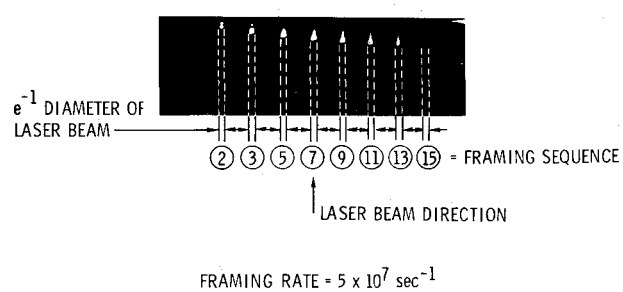

Fig. 10 Framing photographs of breakdown growth (framing rate $2\times 10^7\ s^{-1}$).

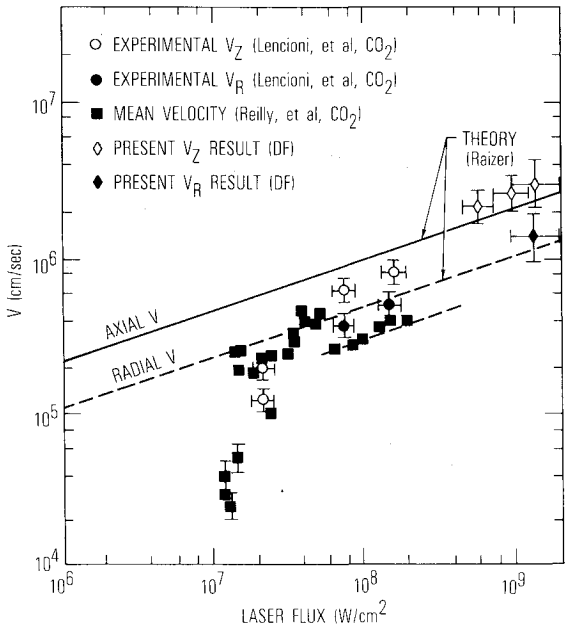

Fig. 11 Plasma growth rate for laser-irradiated aerosols.

aerosol-induced plasmas becomes important. Consider a uniform 55 MW/cm^2, 2 μs (square) pulse propagating through a typical maritime aerosol distribution for which[14]

$$N\,(>10\ \mu\text{m}) = \int_{10\ \mu\text{m}}^{\infty} r^{-5}\,dr = 2.5\times 10^{-5}\ \text{cm}^{-3}$$

and assume a 1 km transmission path of unit area (1 cm^2). In this volume there will be two or three particles with radii of 10 μm or larger. By Fig. 8, a 55 MW/cm^2 beam will produce two or three breakdowns in the subject volume according to the present breakdown theory. At this intensity, the radial expansion velocity is estimated from LSD theory[17] to be

$$v_r = 0.5\left[(\gamma^2-1)(2I_0/\rho_0)\right]^{\frac{1}{3}} = 0.5\ \text{cm}/\mu\text{s} \qquad (6)$$

The time for breakdowns to first develop is estimated from Fig. 9 to be 0.2 μs. Since the breakdowns are assumed to originate near the centerline of the spatially uniform beam, the beam becomes fully blocked about 1 μs after the onset of plasma formation. The fractional energy transmission through the breakdown region can be written as

$$\frac{E_t}{E_i} = \left\{\int_0^{\tau_B} I_0\,dt + \int_{\tau_B}^{\tau_c} I_0\left[1-(v_r t)^2/r_0^2\right]dt\right\}\Big/\int_0^{\tau_v} I_0\,dt$$

$$= \frac{\tau_B}{\tau_v} + \frac{1}{\tau_v}\left[(\tau_c-\tau_B) - \frac{v_r^2}{3r_0^2}\left(\tau_c^3-\tau_B^3\right)\right] \qquad (7)$$

where τ_B is the onset time for breakdown formation, τ_c the beam cutoff time, τ_v the laser pulse duration, and r_0 the beam radius. Equation (7) predicts a fractional energy transmission of 31% for the present example. The generalization to nonuniform spatial and temporal beam profiles is easily accommodated. Note that the above calculation relies on a *theoretical* breakdown threshold estimate for 20 μm diam water aerosols. Since the present theory may underestimate breakdown thresholds for water aerosols of larger diameter ($\geq$ 20 μm), the fractional energy transmission may exceed the value calculated in the present example. Threshold measurements for intermediate- and large-diameter water aerosols are needed to facilitate reliable predictions of long-path transmission in maritime environments.

Conclusions

Pulsed DF chain-laser breakdown thresholds have been investigated in water-particle-laden air. Thresholds for fresh- and salt-water aerosols of small (1-4 μm) diam were measured to lie in the range 0.6-1.8 GW/cm^2. The apparent large spread in the measured small-particle thresholds was explained on the basis of major differences in laser pulse shapes for two different classes of experiments that were performed. Steeply rising pulses yielded thresholds that were 2.5-3 times greater than the breakdown values observed for flat-topped pulses. Collimated DF beams that encountered large-diameter water particles were incapable of producing breakdowns at intensity levels of 50-59 MW/cm^2 and pulse lengths of 0.5 μs. Based on threshold scaling as $\tau_v^{-0.5}$, we postulate a safe intensity for a $t(\mu\text{s})$ duration pulse propagating through 100 μm diam water particles to be $35[t(\mu\text{s})]^{-0.5}$ MW/cm^2.

Confidence in the present experimental technique was increased by conducting threshold measurements using 20 μm diam alumina particles; the wavelength-scaled HF- and CO_2-laser data of Lencioni et al. have been shown to be in excellent agreement with our alumina threshold measurements. A first attempt was made to construct an empirical correlation of DF breakdown threshold as a function of particle size and time-to-breakdown. In this correlation, the present data appear compatible with our wavelength scaling of the short- and long-pulse data of Lencioni et al. and with clean-air breakdown data of Deka et al.

Plasma growth rate measurements for DF irradiated aerosols have been shown to agree with the theoretical predictions of Raizer and are found to be consistent with extrapolations to higher fluences of earlier measurements at CO_2 wavelengths. A plasma temperature of 4.2 eV was inferred from measurements of the axial LSD wave speed at incident intensities in the neighborhood of 1 GW/cm^2. An approximate theoretical model of the aerosol breakdown process was described that was shown to be in reasonable agreement with the experimental DF data. This model allows scaling of the present laboratory-scale results to long transmission paths in maritime environments. To establish greater confidence in this scaling, we propose that additional measurements, using a larger energy DF laser, are needed to obtain breakdown thresholds for intermediate-size (10-40 μm diam) water particles.

Acknowledgment

This work was supported in part by the Naval Research Laboratory/ONR under the U.S. Air Force Space Division, Contract F04701-81-C-0082.

References

[1]Smith, D.C., "Gas Breakdown Dependence on Beam Size and Pulse Duration with 10.6 Micron Radiation," *Applied Physics Letters*, Vol. 19, Nov. 1971, pp. 405-407.

[2]Canavan, G.H., Proctor, W.A., Nielsen, P.E., and Rockwood, S.D., "CO_2 Laser Air Breakdown Calculations," *IEEE Journal of Quantum Electronics*, Vol. 8, Jan. 1972, pp. 564-572.

[3]Canavan, G.H. and Nielsen, P.E., "Focal Spot Size Dependence of Gas Breakdown Induced by Particulate Ionization," *Applied Physics Letters*, Vol. 22, April 1973, pp. 409-410.

[4]Lencioni, D.E., "The Effect of Dust on 10.6 Micron Laser-Induced Air Breakdown," *Applied Physics Letters*, Vol. 23, July 1973, pp. 12-14.

[5]Lencioni, D.E., "Laser-Induced Air Breakdown for 1.06 Micron Radiation," *Applied Physics Letters*, Vol. 25, July 1974, pp. 15-17.

[6]Smith, D.C. and Brown, R.T., "Aerosol-Induced Air Breakdown with CO_2 Laser Radiation," *Journal of Applied Physics*, Vol. 46, March 1975, pp. 1146-1155.

[7]Reilly, J.P., Singh, P., and Weyl, G., "Multiple Pulse Propagation in Fog, Rain and Dust at 10.6 Microns," Avco Everett Research Laboratory, Interim Report for Period Sept. 1975 to April 1976, July 1976.

[8]Lencioni, D.E., Pettingill, L.C., and DeGloria, D.P., "Air Breakdown Initiated by Particles in an HF Laser Beam," MIT Lincoln Laboratory, Rept. LTP-35, Oct. 1976.

[9]Bunkin, F.V. and Savranskii, V.V., "Optical Breakdown of Gases Induced by the Thermal Explosion of Suspended Microscopic Particles," *Soviet Physics—JETP*, Vol. 38, June 1974, pp. 1091-1096.

[10]Nichols, D.B. and Hall, R.B., "Helium Breakdown by DF Laser Radiation," *Journal of Applied Physics*, Vol. 52, June 1981, pp. 3851-3854.

[11]Deka, B.K., Dyer, P.E., James, D.J., and Ramsden, S.A., "Gas Breakdown Threshold Measurements Using a Pulsed HF/DF Laser," *Optics Communications*, Vol. 19, Nov. 1976, pp. 292-296.

[12]Soileau, M.J., "Air Breakdown by Pulsed Laser Radiation in the 2.7 and 3.8 Micron Region," *Applied Physics Letters*, Vol. 35, Aug. 1979, pp. 309-311.

[13]Amimoto, S.T., Whittier, J.S., Lundquist, M.L., Ronkowski, F.G., Ortwerth, P.J., and Hofland, R., "Pulsed Chemical Laser with Variable Pulse-Length E-Beam Initiation and Magnetic Confinement," *Applied Physics Letters*, Vol. 40, Jan. 1982, pp. 20-23.

[14]Trusty, G.L. and Cosden, T.H., "Optical Extinction Predictions from Measurements in the Open Sea," Naval Research Laboratory, Rept. 8260, Jan. 1979.

[15]Hofland, R., "Pulsed Laser Propagation Through Aerosol Breakdowns: Simple Model," Aerospace Corp., Rept. ATM-81(6720)-1, April 1981.

[16]Smith, D.C., "Gas Breakdown Initiated by Laser Radiation Interaction with Aerosols and Solid Surfaces," *Journal of Applied Physics*, Vol. 48, June 1977, pp. 2217-2225.

[17]Raizer, Y.P., "Heating of a Gas by a Powerful Light Pulse," *Soviet Physics—JETP*, Vol. 21, March 1965, pp. 1009-1017.

[18]Reilly, J., Singh, P., and Weyl, G., "Multiple Pulse Laser Propagation Through Atmospheric Dusts at 10.6 Microns," AIAA Paper 77-697, June 1977.

[19]Larkin, A.I., "Thermodynamic Functions of a Low Temperature Plasma," *Soviet Physics—JETP*, Vol. 11, Dec. 1960, pp. 1363-1367.